Human motion estimation on Lie groups using IMU measurements

Vladimir Joukov*, Josip Ćesić‡, Kevin Westermann*, Ivan Marković‡, Dana Kulić* and Ivan Petrović‡

***Abstract*— This paper proposes a new algorithm for human motion estimation using inertial measurement unit (IMU) measurements. We model the joints by matrix Lie groups, namely the special orthogonal groups $\mathsf{SO}(2)$ and $\mathsf{SO}(3)$, representing rotations in 2D and 3D space, respectively. The state space is defined by the Cartesian product of the rotation groups and their velocities and accelerations, given a kinematic model of the articulated body. In order to estimate the state, we propose the Lie Group Extended Kalman Filter (LG-EKF), thus explicitly accounting for the non-Euclidean geometry of the state space, and we derive the LG-EKF recursion for articulated motion estimation based on IMU measurements. The performance of the proposed algorithm is compared to the EKF based on Euler angle parametrization in both simulation and real-world experiments. The results show that the proposed filter is a significant improvement over the Euler angles based EKF, since it estimates motion more accurately and is not affected by gimbal lock.**

I. Introduction

Human motion measurement is a key enabling technology in many applications, including human motion analysis, rehabilitation, imitation learning and human-robot interaction [1]. A number of different sensing modalities have been proposed for human motion measurement, including camera, magnetic and wearable systems [1]. When line of sight between the sensor and the human cannot be ensured, and when motion is to be captured in large or outdoor spaces, wearable sensing, based on inertial measurement units (IMUs) is preferred.

Many previous works focus on human pose estimation using wearable IMUs. A simple approach is to integrate the gyroscope to estimate the orientation of each limb, however, due to gyroscope drift error accumulates over time [2]. Stochastic filter methods are often used to combine gyroscope and accelerometer signals to reduce drift and allow for estimation of highly dynamic motions. Without taking into account the kinematic model of the human body, the orientation of each limb can be estimated separately [3], [4] with the Kalman filter. In post processing kinematic constraints can be incorporated and the joint angle estimated via optimization [5].

This work has been supported from the Unity Through Knowledge Fund under the project *Cooperative Cloud based Simultaneous Localization and Mapping in Dynamic Environments* (cloudSLAM) and by the Ministry of Science, Education and Sports of the Republic of Croatia under the grant *Center of Research Excellence for Data Science and Cooperative Systems* (CoE ACROSS).

* Vladimir Joukov, Kevin Westermann and Dana Kulić are with the University of Waterloo, Department of Electrical and Computer Engineering, Adaptive Systems Laboratory, Canada. {vjoukov@uwaterloo.ca, kgwester@uwaterloo.ca, dkulic@uwaterloo.ca}

‡ Josip Ćesić, Ivan Marković and Ivan Petrović are with the University of Zagreb, Faculty of Electrical Engineering and Computing, Laboratory for Autonomous Systems and Mobile Robotics, Croatia. {josip.cesic@fer.hr, ivan.markovic@fer.hr, ivan.petrovic@fer.hr}

To retrieve the joint angles directly, human kinematic constraints must be incorporated into the estimation. Steel *et al.* [6] utilized arbitrary leg movement and optimization techniques to extract the constraints and used a weighted combination of the gyroscope integral and accelerometer projected onto the knee joint axis. If the kinematic model is available a priori, stochastic filter methods can be used to directly estimate human pose from IMU measurements. Modeling the human body as a set of rigid links connected with hinge joints Lin and Kulić [7] and El-Gohary and McNames [8] used the Extended and the Unscented Kalman filters to estimate arbitrary 3D leg and arm motion respectively. Model based extended quaternion Kalman filter was used by Szczesna to track a 3-segment inverted pendulum motion [9]. Finally, having a model of the motion in addition to the kinematic constraints can further improve human pose estimation [2], [10].

In most of the aforementioned works the joints of the kinematic model are described using Euler angles and while [9] provides a quaternion joints representation, the approach cannot provide different constraints for human joints with different degrees of freedom (dof): 3 at the hip and shoulder, 2 in the elbow and wrist, and a single dof at the knee. In our previous work [11] we showed that Lie Group based kinematic modeling can correctly represent the degrees of freedom of the human body and that Lie Group based extended Kalman filter can significantly improve camera based pose estimation. A number of other studies have also investigated the uncertainty modelling and representation on Lie groups. In [12]–[14] representation and propagation of uncertainty on Lie groups was studied in the context of manipulator kinematics and camera trajectory estimation, and later in [15] the authors studied the example of a stochastic kinematic model of a differential drive mobile robot on $\mathsf{SE}(2)$. Uncertainty association, propagation and fusion on $\mathsf{SE}(3)$ was investigated in [16]. In [17] the authors preintegrated a number of IMU measurements for visual-inertial navigation by properly addressing the geometry of the rotation group and defining the uncertainty in the pertaining tangent space. Finally, an extended Kalman filter on Lie groups (LG-EKF) was proposed in [18], [19] and has been further developed to an iterative version [20].

In this paper we propose a novel approach for human motion estimation based solely on IMU measurements. The proposed filtering approach performs stochastic inference of human motion by defining the state space to reside on a Lie group, with each state element corresponding to the kinematic model of the analysed human body part. Then, the LG-EKF is derived, where the prediction step is based on the constant acceleration model [21], while the

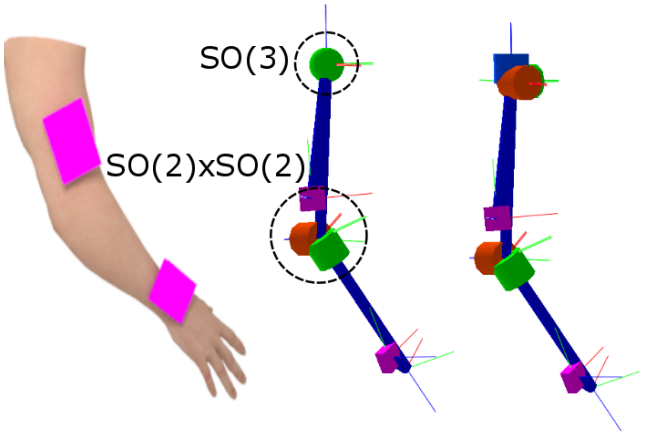

Fig. 1: Left: 3D Arm model showing simulation IMU placement. Middle: Lie group-based arm model with attached IMU units for dynamic motion simulation. Right: Euler angle-based arm model.

update step depends on the gyro and accelerometer measurements of the IMU units. We compare the performance of the proposed algorithm with an EKF based on the Euler angles parametrization both in simulation and real-world experiments. The results show that the proposed approach significantly improves performance and is not affected by gimbal lock.

The rest of the paper is organised as follows. In Section II we present the mathematical fundamentals addressing Lie groups and associated uncertainties. In Section III we present the novel LG-EKF, while in Section IV we briefly describe the EKF based on Euler angles. Section V presents the validation results and Section VI concludes the paper.

II. Mathematical Background

In this section we provide the mathematical background for human motion estimation on matrix Lie groups. Our human body modeling approach and the corresponding state space construction is the same as proposed in [22], which we briefly review for the completeness.

A. Construction of the state space

We construct the state space by using Lie group representatives for each joint of interest. As an example we consider a state space model of a human arm from shoulder to wrist employing Lie groups, as illustrated in Fig. 1.

An example of group G representing the state space for this model is

$$\mathsf{G} = \overbrace{\mathsf{SO}(3)}^{\text{shoulder}} \times \overbrace{\mathsf{SO}(2) \times \mathsf{SO}(2)}^{\text{elbow}} . \tag{1}$$

The first element in (1) describes the shoulder employing a special orthogonal group $\mathsf{SO}(3)$ and providing 3 DoF mobility, while the second and third elements jointly model the 2 DoF motion of the flexion/extension and internal rotation of the elbow joint, where each element of a special orthogonal group $\mathsf{SO}(2)$ contributes a single DoF. Note that the choice of the state space only incorporates system variables and not the full forward kinematics.

B. Lie groups and Lie algebra

A Lie group G is a group which also has the structure of a smooth manifold. The group operators, composition and inversion, are smooth operations. Each point $X \in \mathsf{G}$ has an associated tangent space $T_X(\mathsf{G})$ [23]. This linear tangent space is usually placed at the group identity, and is called the Lie algebra of G, which we denote by $\mathfrak{g}$ [24]. The Lie algebra $\mathfrak{g}$, which is of the same dimension as G, admits a binary operation $[\cdot,\cdot]$ called the Lie bracket, which reflects the non-commutative content of the group operation. Furthermore, if the group G is a matrix Lie group, then $\mathsf{G} \subset \mathbb{R}^{n\times n}$ and group operations are simply matrix multiplication and inversion.

The Lie algebra $\mathfrak{g} \subset \mathbb{R}^{n\times n}$ associated to a p-dimensional matrix Lie group $\mathsf{G} \subset \mathbb{R}^{n\times n}$ is a p-dimensional vector space defined by a basis consisting of p real matrices E_r, $r = 1,\ldots,p$, often referred to as generators [25]. In particular, a Lie algebra is an open neighbourhood around $\mathbf{0}^p$ in the tangent space of G at the identity $\boldsymbol{I}^n$. The matrix exponential $\exp_{\mathsf{G}}$ and matrix logarithm $\log_{\mathsf{G}}$ establish a local diffeomorphism between G and $\mathfrak{g}$ as

$$\exp_{\mathsf{G}} : \mathfrak{g} \to \mathsf{G} \quad \text{and} \quad \log_{\mathsf{G}} : \mathsf{G} \to \mathfrak{g}. \tag{2}$$

Furthermore, a natural relation exists between the p-dimensional Lie algebra $\mathfrak{g}$ and the Euclidean space $\mathbb{R}^p$, and is given through a linear isomorphism

$$[\cdot]_{\mathsf{G}}^{\vee} : \mathfrak{g} \to \mathbb{R}^p \quad \text{and} \quad [\cdot]_{\mathsf{G}}^{\wedge} : \mathbb{R}^p \to \mathfrak{g}. \tag{3}$$

For brevity, we will use the following notation [20]

$$\exp_{\mathsf{G}}^{\wedge}(x) = \exp_{\mathsf{G}}([x]_{\mathsf{G}}^{\wedge}) \quad \text{and} \quad \log_{\mathsf{G}}^{\vee}(X) = [\log_{\mathsf{G}}(X)]_{\mathsf{G}}^{\vee}, \tag{4}$$

where $x \in \mathbb{R}^p$ and $X \in \mathsf{G}$.

Since Lie groups are generally non-commutative, i.e., $XY \neq YX$, we also need to employ the adjoint representations. The adjoint representation of G on $\mathfrak{g}$, Ad_{G}, can be seen as as a way of representing the elements of the group as a linear transformation of the group's algebra, and in general, it measures the failure of $X \in \mathsf{G}$ to commute with elements of G near the identity [26]. The adjoint representation of $\mathfrak{g}$, ad_{G}, is in fact the differential of Ad_{G} at the identity element. For a commutative group, the map ad evaluates to zero.

C. Concentrated Gaussian distribution

To make use of EKF on Lie groups, we need to establish first a notion of a Gaussian distribution on Lie groups. A distribution on a Lie group that is tightly focused, meaning that almost all the mass of the distribution is concentrated in a small neighborhood around the mean, can be expressed in the Lie algebra [16], [27], and this concept is called a concentrated Gaussian distribution.

Let $X \in \mathsf{G}$ be a random variable following a concentrated Gaussian distribution with mean μ and covariance P as

$$X = \mu \exp_{\mathsf{G}}^{\wedge}(\epsilon), \quad X \sim \mathcal{G}(\mu, P), \tag{5}$$

where $\epsilon \sim \mathcal{N}_{\mathbb{R}^p}(\mathbf{0}^p, P)$ is a zero-mean Gaussian distribution with covariance $P \subset \mathbb{R}^{p\times p}$ defined in the Lie algebra, i.e., the Euclidean space $\mathbb{R}^p$. We can see form (5) that the mean value μ is defined on G, while the associated uncertainty resides in $\mathbb{R}^p$. Roughly, this concept allows us to work with the covariance directly in $\mathbb{R}^p$ and use Euclidean tools, almost as we would with a 'classical' Gaussian distribution [19]. For a more formal introduction of the concepts presented here, the interested reader is referred to [28].

D. Special orthogonal groups $\mathsf{SO}(2)$ and $\mathsf{SO}(3)$

The special orthogonal group $\mathsf{SO}(n)$ is the matrix group

$$\mathsf{SO}(n) = \left\{ X \subset \mathbb{R}^{n\times n} \,|\, X^{\mathrm{T}}X = I,\, \det(X) = 1 \right\}. \quad (6)$$

For $n = 2, 3$ this group defines rotations in 2D and 3D, respectively. The algebra $\mathfrak{so}(n)$ comprises of $n \times n$ skew-symmetric matrices. For Euclidean vectors $x = \phi$ and $x = [\phi_1\ \phi_2\ \phi_3]^{\mathrm{T}}$, the algebras $\mathfrak{so}(2)$ and $\mathfrak{so}(3)$ amount to

$$x^{\wedge}_{\mathsf{SO}(2)} = \begin{bmatrix} 0 & -\phi \\ \phi & 0 \end{bmatrix},\ x^{\wedge}_{\mathsf{SO}(3)} = \begin{bmatrix} 0 & -\phi_3 & \phi_2 \\ \phi_3 & 0 & -\phi_1 \\ -\phi_2 & \phi_1 & 0 \end{bmatrix}, \quad (7)$$

where $(\cdot)^{\wedge}_{\mathsf{SO}(n)} : \mathbb{R}^n \to \mathfrak{so}(n)$, while its inverse, $(\cdot)^{\vee}_{\mathsf{SO}(n)} : \mathfrak{so}(n) \to \mathbb{R}^n$, follows trivially from (7).

For $\mathsf{SO}(2)$, the exponential map yields the classical 2D rotation matrix, while the logarithm evaluates to simple extraction of ϕ into a skew-symmetric matrix form in (7). Since $\mathsf{SO}(2)$ is commutative, its adjoint representations are trivial: $\mathrm{Ad}_{\mathsf{SO}(2)}$ is a unit map and $\mathrm{ad}_{\mathsf{SO}(2)}$ is zero. The exponential for $\mathsf{SO}(3)$, performing mapping $\exp_{\mathsf{SO}(3)} : \mathfrak{so}(3) \to \mathsf{SO}(3)$, is given as

$$\begin{aligned} \exp^{\wedge}_{\mathsf{SO}(3)}(x) =& \cos(|x|)I^3 + \\ &+ (1 - \cos(|x|))\frac{xx^{\mathrm{T}}}{|x|^2} + \sin(|x|)\frac{x^{\wedge}_{\mathsf{SO}(3)}}{|x|}. \end{aligned} \quad (8)$$

The logarithm, performing mapping $\log_{\mathsf{SO}(3)} : \mathsf{SO}(3) \to \mathfrak{so}(3)$, is given as

$$\begin{aligned} \log_{\mathsf{SO}(3)}(X) &= \frac{\theta}{2\sin(\theta)}(X - X^{\mathrm{T}}) \\ \text{s.t.} \quad & 1 + 2\cos(\theta) = \mathrm{Tr(X)} \\ & \begin{cases} \theta \neq 0 & -\pi < \theta < \pi \\ \theta = 0 & \log(X) = 0 \end{cases}. \end{aligned} \quad (9)$$

The adjoints $\mathrm{Ad}_{\mathsf{SO}(3)}$ and $\mathrm{ad}_{\mathsf{SO}(3)}$ are respectively given as

$$\mathrm{Ad}_{\mathsf{SO}(3)}(X) = X \text{ and } \mathrm{ad}_{\mathsf{SO}(3)}(x) = x^{\wedge}_{\mathsf{SO}(3)}. \quad (10)$$

In the sequel we present the new human motion estimation method based on the LG-EKF using IMU measurements.

III. Human motion estimation on Lie groups

A. Motion prediction step

We assume that the motion model of the system can be described with the following equation [19]

$$X_{k+1} = f(X_k, n_k) = X_k \exp^{\wedge}_{\mathsf{G}}\left(\hat{\Omega}_k + n_k\right), \quad (11)$$

where $X_k \in \mathsf{G}$ is the state of the system at time k, G is a p-dimensional Lie group, $n_k \sim \mathcal{N}_{\mathbb{R}^p}(\mathbf{0}^{p\times 1}, Q_k)$ is zero mean white Gaussian noise with covariance Q_k, and $\hat{\Omega}_k = \Omega(X_k) : \mathsf{G} \to \mathbb{R}^p$ is a non-linear $\mathcal{C}^2$ function.

In our approach, similar to our previous work [22], we assume the human motion to follow a constant acceleration model and our state space G is then constructed to include the positional, velocity and acceleration components block-diagonally. Hence exponentials and logarithms will keep the state in the block diagonal arrangement as well. The motion model of a single joint i is given as

$$\hat{\Omega}^i_k = \begin{bmatrix} \mathrm{T}\omega^i_k + \frac{\mathrm{T}^2}{2}\alpha^i_k \\ \mathrm{T}\alpha^i_k \\ 0 \end{bmatrix} \in \mathbb{R}^{3\mathrm{d}_i}, n_k = \begin{bmatrix} \frac{\mathrm{T}^2}{2}n^i_k \\ \mathrm{T}n^i_k \\ n^i_k \end{bmatrix} \in \mathbb{R}^{3\mathrm{d}_i} \quad (12)$$

where ω^i_k and α^i_k are the angular velocity and angular acceleration represented in the Lie algebra[1]. The term n^i_k represents the acceleration increment during the k-th sampling period [29], and d_i represents the number of DoFs of the i-th joint.

Given that the posterior distribution at step k follows the concentrated Gaussian distribution $\mathcal{G}(\mu_k, P_k)$, and following the LG-EKF prediction step [22], the resulting prediction can be approximated with a concentrated Gaussian distribution $\mathcal{G}(\mu_{k+1|k}, P_{k+1|k})$. The mean propagation of the LG-EKF is governed by

$$\mu_{k+1|k} = \mu_k \exp^{\wedge}_{\mathsf{G}}\left(\hat{\Omega}_k\right), \quad (13)$$

while the covariance prediction is computed as

$$P_{k+1|k} = \mathcal{F}_k P_k \mathcal{F}_k^{\mathrm{T}} + \Phi_{\mathsf{G}}(\hat{\Omega}_k) Q_k \Phi_{\mathsf{G}}(\hat{\Omega}_k)^{\mathrm{T}}. \quad (14)$$

The operator $\mathcal{F}_k$ can be seen as a matrix Lie group equivalent to the Jacobian of $f(X_k, n_k)$, and is calculated by

$$\begin{aligned} \mathcal{F}_k &= \mathrm{Ad}_{\mathsf{G}}\left(\exp^{\wedge}_{\mathsf{G}}\left(-\hat{\Omega}_k\right)\right) + \Phi_{\mathsf{G}}(\hat{\Omega}_k)\mathscr{L}_k \\ \mathscr{L}_k &= \frac{\partial}{\partial \epsilon}\Omega\left(\mu_k \exp^{\wedge}_{\mathsf{G}}(\epsilon)\right)_{|\epsilon=0}. \end{aligned} \quad (15)$$

The term $\mathscr{L}_k$ represents the linearisation term where the argument of the motion model is the mean of the current state X_k with an incremental perturbation additively added in each of the p directions. Contrary to the conventional EKF, a linear additive process noise affects the system as a function of the current state of the system over the transformation

[1]Euclidean space $\mathbb{R}^p, p \in \mathbb{N}$ is a matrix Lie group and in order to construct G we employ its matrix representation obtained by simple matrix embedding. The matrix representation of the Euclidean space is also a subgroup of $\mathsf{SE}(n)$ where a pure translation is employed [28].

$\Phi_{\mathsf{G}}(\hat{\Omega}_k) Q_k \Phi_{\mathsf{G}}(\hat{\Omega}_k)^{\mathrm{T}}$, where Φ_{G} appears due to the displacement of the tangential space during the prediction step, and is given by

$$\Phi_{\mathsf{G}}(v) = \sum_{i=0}^{\infty} \frac{(-1)^i}{(i+1)!} \operatorname{ad}_{\mathsf{G}}(v)^i \,, \; v \in \mathbb{R}^p \,. \tag{16}$$

B. Measurement update step

We next derive the update step by employing gyro and accelerometer measurements of IMUs attached to a human body. The discrete measurement model on the matrix Lie group is modelled as

$$Z_{k+1} = h(X_{k+1}) \, \exp^{\wedge}_{\mathsf{G}'} (m_{k+1}) \,, \tag{17}$$

where $Z_{k+1} \in \mathsf{G}'$, $h : \mathsf{G} \to \mathsf{G}'$ is a $\mathcal{C}^1$ function, G' is a p'-dimensional Lie group and $m_{k+1} \sim \mathcal{N}_{\mathbb{R}^q}(\mathbf{0}^{q\times 1}, R_{k+1})$ is zero-mean white Gaussian noise with covariance R_{k+1}. The update step of the filter strongly resembles the standard EKF update procedure, relying on the Kalman gain K_{k+1} and innovation vector ν_{k+1} calculated as

$$\begin{aligned} K_{k+1} &= P_{k+1|k} \mathcal{H}_{k+1}^{\mathrm{T}} \left(\mathcal{H}_{k+1} P_{k+1|k} \mathcal{H}_{k+1}^{\mathrm{T}} + R_{k+1} \right)^{-1} \\ \nu_{k+1} &= K_{k+1} \log^{\vee}_{\mathsf{G}'} \left(h(\mu_{k+1|k})^{-1} Z_{k+1} \right) \,. \end{aligned} \tag{18}$$

The matrix $\mathcal{H}_{k+1}$ can be seen as the matrix Lie group equivalent of the Jacobian of $h(X_{k+1})$, and is given as

$$\mathcal{H}_{k+1} = \frac{\partial}{\partial \epsilon} \log^{\vee}_{\mathsf{G}'} \left(h(\mu_{k+1|k})^{-1} h(\mu^{\epsilon}_{k+1|k}) \right)_{|\epsilon=0} \,,$$

where $h(\mu^{\epsilon}_{k+1|k}) = h(\mu_{k+1|k} \exp^{\wedge}_{\mathsf{G}}(\epsilon))$, describes the variation of measurements for an infinitesimal motion ϵ. We now evaluate the matrix $\mathcal{H}_{k+1}$ based on gyro and accelerometer measurements.

C. Gyro update

The measurement function of the gyro measurement is:

$$h(X_{k+1|k}) = \sum_{i=1}^{n} \mathcal{K}_s^{i,R} \, \omega^i_{k+1|k} \,, \tag{19}$$

where n is the number of joints preceding the gyro sensor s. The term $\mathcal{K}_s^{i,R} = \mathcal{K}_s^{i,R}(X_{k+1|k})$ stands for the rotational component of the forward kinematics between the i-th joint and the gyro sensor s, thus affecting its measurement [30]. The gyro measurements are affected by position (through kinematics) and velocity, hence the corresponding parts of $\mathcal{H}_{k+1}$ matrix need to be evaluated.

By applying partial derivatives and evaluating the multivariate limits similarly to [31], the part of $\mathcal{H}_{k+1}$ relating the gyro measurement to the orientation of the l-th joint $\mathcal{H}^{\theta,l}_{k+1}$ is given as:

$$\mathcal{H}^{\theta,l,r}_{k+1} = \sum_{i=1}^{l} \mathcal{K}_l^{i,R} \theta^l_{k+1|k} E^{l,r} \mathcal{K}_s^{l,R} \omega^i_{k+1|k} \,, \tag{20}$$

where $\mathcal{K}_l^{i,R}$ represents the rotation between the i-th and l-th joint, $\theta^l_{k+1|k}$ is the position of the l-th joint, while $E^{l,r}$ represents the r-th generator of a Lie group representing the l-th joint [27]. Each of the generators represents an infinitesimal motion in one of the directions of a Lie group.

The part of $\mathcal{H}_{k+1}$ relating the gyro measurement to the velocity of the l-th joint $\mathcal{H}^{\omega,l}_{k+1}$ is given as:

$$\mathcal{H}^{\omega,l}_{k+1} = \mathcal{K}_s^{l,R} \,. \tag{21}$$

Since gyro measurement (19) is not a function of the joint accelerations, the part of the $\mathcal{H}_{k+1}$ matrix relating gyro measurements to l-th joint acceleration components is filled with zero values; $\mathcal{H}^{\alpha,l}_{k+1} = 0$.

D. Accelerometer update

The measurement function corresponding to the accelerometer measurement is:

$$h(X_{k+1|k}) = \overbrace{\mathcal{K}_0^{s,R} \ddot{p}_{k+1|k}}^{\text{point acceleration}} + \overbrace{\mathcal{K}_0^{s,R} g}^{\text{gravity component}} \,, \tag{22}$$

where the first term emerges due to dynamics of a body, while the second term arises due to gravity. The superscript R denotes that only the rotation part is embedded into an $\mathsf{SE}(3)$ member, while the translation part is set to 0. The term $\ddot{p}_{k+1|k}$ represents an acceleration of the sensor s represented in the base frame and given in homogeneous coordinates, while g is the gravity vector in homogeneous coordinates. In order to evaluate $\ddot{p}_{k+1|k}$, we start from defining the IMU position as

$$p_{k+1|k} = \mathcal{K}_s^0 \mathcal{O} \tag{23}$$

where $\mathcal{O} = [0 \;\; 0 \;\; 0 \;\; 1]^{\mathrm{T}}$ is the origin represented in homogeneous coordinates. The forward kinematics can be decomposed as

$$\mathcal{K}_s^0 = T_1^0 \theta^1_{k+1|k} T_2^1 \theta^2_{k+1|k} \cdots T_n^{n-1} \theta^n_{k+1|k} \tag{24}$$

Each part of the forward kinematics $\mathcal{K}_i^{i-1} = T_i^{i-1} \theta^i_{k+1|k}$ consists of the constant transformation T_i^{i-1} and the position of the i-th joint $\theta^i_{k+1|k}$. In order to sequentially apply a matrix multiplication inducing each joint state, we describe joints as 4×4 transformation matrices (in terms of Lie groups denoted as special euclidean group $\mathsf{SE}(3)$). We now evaluate the first two derivatives of sensor position $p_{k+1|k}$. The velocity of the point $p_{k+1|k}$ evaluates to

$$\dot{p}_{k+1|k} = \sum_{i=1}^{n} \left(\mathcal{K}_i^0 S^{i,\omega}_{k+1|k} \mathcal{K}_s^i \right) \mathcal{O} \,, \tag{25}$$

where the summation iterates over n joints affecting sensor s, while the term $S^{i,\omega}_{k+1|k}$ is given as

$$S^{i,\omega}_{k+1|k} = \sum_{r=1}^{d_i} \left(\omega^{i,r}_{k+1|k} E^{i,r} \right) , \tag{26}$$

which is a function of the number of degrees of freedom d_i of the i-th joint, and the superscript ω denotes that the

velocity components are summed up. The acceleration of the point $p_{k+1|k}$ evaluates to

$$\ddot{p}_{k+1|k} = \overbrace{\sum_{i=1}^{n}\left(\sum_{j=1}^{i}\left(\mathcal{K}_j^0 S_{k+1|k}^{j,\omega}\mathcal{K}_i^j\right)S_{k+1|k}^{i,\omega}\mathcal{K}_s^i\right)\mathcal{O}}^{\text{centripetal force component I}} + \quad (27)$$

$$\overbrace{\sum_{i=1}^{n}\left(\mathcal{K}_i^0 S_{k+1|k}^{i,\omega}\sum_{j=i+1}^{n}\left(\mathcal{K}_j^i S_{k+1|k}^{j,\omega}\mathcal{K}_s^j\right)\right)\mathcal{O}}^{\text{centripetal force component II}} +$$

$$\underbrace{\sum_{i=1}^{n}\left(\mathcal{K}_i^0 S_{k+1|k}^{i,\alpha}\mathcal{K}_s^i\right)\mathcal{O}}_{\text{joint acceleration component}} .$$

The acceleration $\ddot{p}_{k+1|k}$ consists of two components – the centripetal force component and joint acceleration component, which we emphasize in (27).

We now proceed to linearize and evaluate the part of $\mathcal{H}_{k+1}$ corresponding to the accelerometer measurement and joint l. It is given as

$$\begin{bmatrix}\mathcal{H}_{k+1}^l \\ 1\end{bmatrix} = \frac{\partial \mathcal{K}_0^{s,R}}{\partial X_{k+1|k}^l}\left(\ddot{p}_{k+1|k}+g\right) + \mathcal{K}_0^{s,R}\frac{\partial \ddot{p}_{k+1|k}}{\partial X_{k+1|k}^l} . \quad (28)$$

In order to evaluate (28) we need to compute partial derivatives of $\mathcal{K}_0^{s,R}$ and $\ddot{p}_{k+1|k}$ with respect to position, velocity, and acceleration of $X_{k+1|k}^l$. We omit the detailed derivation for brevity; for completeness we provide them in the supplementary material available at [32].

Finally, having evaluated $\mathcal{H}_{k+1}$, the measurement update step is calculated as [19]

$$\begin{aligned}\mu_{k+1} &= \mu_{k+1|k}\exp_{\mathsf{G}}^{\wedge}(\nu_{k+1}) \quad (29)\\ P_{k+1} &= \Phi_{\mathsf{G}}(\nu_{k+1})\left(I - K_{k+1}\mathcal{H}_{k+1}\right)P_{k+1|k}\Phi_{\mathsf{G}}(\nu_{k+1})^{\mathrm{T}} .\end{aligned}$$

IV. Euler Angle Based Approach

The proposed approach is compared to a conventional EKF applied to a standard kinematic model defined with revolute and prismatic joints [33]. Three perpendicular revolute joints (Euler angles) can be used to model human spherical joints such as the shoulder and the hip. The state of the EKF is defined as the position q, velocity $\dot{q}$, and acceleration $\ddot{q}$ of the joints. Assuming constant acceleration the linear motion model is

$$\begin{aligned}q_{k+1} &= q_k + T\dot{q}_k + \frac{T^2}{2}\ddot{q}_k\\ \dot{q}_{k+1} &= \dot{q}_k + T\ddot{q}_k \quad (30)\\ \ddot{q}_{k+1} &= \ddot{q}_k .\end{aligned}$$

V. Validation Results

We validate the proposed approach both in simulation and with real human motion. First, in simulation, we demonstrate the benefits of LG-EKF over EKF when using IMU measurements during highly dynamical movements whose motion is better described on the group and show that unlike EKF, LG-EKF is not affected by gimbal lock. Next, we evaluate the performance of LG-EKF and EKF on real IMU data of dynamic figure eight arm movement sequence.

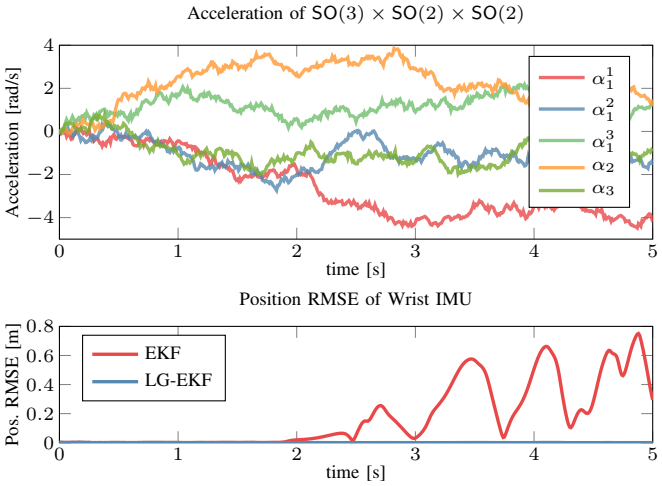

Fig. 2: Performance of EKF and LG-EKF based on Brownian motion on Lie Algebra. Since LG-EKF has an accurate motion model it correctly tracks the arm movement. Once the angular accelerations on the Lie Algebra become large, the constant Euler angle acceleration model of EKF does not provide a good state prediction and EKF cannot maintain an accurate estimate. α_1 denotes $\mathsf{SO}(3)$ with 3 dofs, while α_2 and α_3 correspond to $\mathsf{SO}(2)$ joints with a single dof.

A. Simulation Validation

1) Dynamic Motion: To test the properties of LG-EKF, we simulate a human arm composed of the shoulder and elbow joints, where the state is an element of $\mathsf{SO}(3) \times \mathsf{SO}(2) \times \mathsf{SO}(2)$ composition. Two IMUs are attached to the humerus and radius at offsets of $[0.1\,0.1\,0.3]^{\mathrm{T}}$, and $[0.1\,0.1\,0.4]^{\mathrm{T}}$ respectively. The kinematic chain is visualized in Fig. 1.

It is possible to generate Brownian motion either on the group or on Euler angles to exactly match the constant acceleration with zero mean Gaussian noise assumption of LG-EKF or EKF. Since large constant acceleration in one representation implies a quickly changing acceleration in the other, we can expect the filter with the correct motion model to significantly outperform the other in high acceleration regions. Figure 2 shows the Brownian motion generated on the group representation of the arm and the error in position estimation of the wrist IMU for EKF and LG-EKF. It is clear that during high constant accelerations on the group, Euler angle based EKF cannot accurately track the motion.

However, it is unlikely that human motion will exactly follow one motion model or the other. Thus, in order to compare EKF and LG-EKF without being biased to a specific motion representation we generate a dynamic trajectory in task space and utilize inverse kinematics to recover joint angles of the Euler angle model. Next we numerically differentiate the trajectory to retrieve joint velocities and accelerations and generate the IMU measurements using forward kinematics. The task space trajectory is created by cubic splining points in the reachable workspace generated from a univariate distribution. This setup creates a highly dynamic motion as can be seen from the positions of the

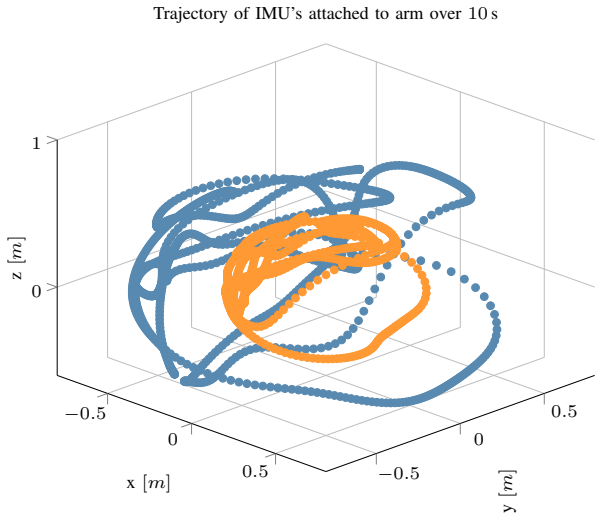

Fig. 3: 10 Second simulation trajectory of the IMUs attached to the humerus and radial undergoing the generated highly dynamic motion.

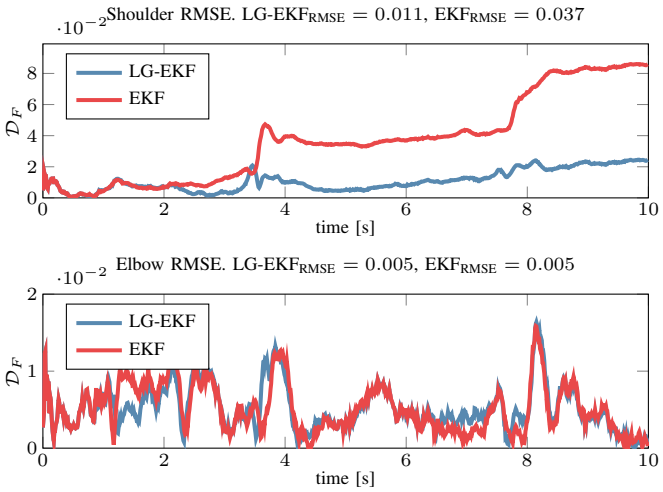

Fig. 4: Error between the actual and estimated rotations at the shoulder and elbow joint for LG-EKF and EKF during task space generated dynamic motion. Estimation of shoulder rotation is significantly improved using the SO(3) model. Due to the improvement in the SO(3) joint we also see a small improvement in the $\mathsf{SO}(2) \times \mathsf{SO}(2)$ joint.

two IMUs shown in Fig. 3. Simulated IMUs are sampled at 100 Hz and zero mean Gaussian noise with standard deviations of $0.01\frac{rad}{s}$ and $0.1\frac{m}{s^2}$ is added to the gyroscope and accelerometer measurements respectively. For both filters the initial covariances were set to diagonal matrix of a 10^{-3} denoting accurate knowledge of the initial state. The process noise was assumed to follow the discrete constant acceleration process noise injection. For each triplet $[\phi\ \omega\ \alpha]$ or $[q\ \dot{q}\ \ddot{q}]$ noise of standard deviation η is injected into α and is propagated to ω and ϕ by integration. Thus, for each triplet the process noise covariance is GG^T where $G = [\frac{T^2}{2}\ T\ 1]\eta$. For the dynamic motion simulation η was set to $10\frac{rad}{s^2}$ per iteration. The observation noise was set to the true sensor noise values.

To compare the estimate with the ground truth, we use the deviation from the identity matrix as the distance metric [34]

$$\mathcal{D}_F = \left\| I - R_e^{\mathrm{T}} R_{gt} \right\|_F \tag{31}$$

where R_e and R_{gt} are the estimated and ground truth rotation matrices of each joint and $\|\cdot\|_F$ denotes the Frobenius norm.

Figure 4 shows the comparison between the LG-EKF and EKF using this distance metric for the shoulder and elbow joints. The LG-EKF significantly outperforms the EKF filter, which is due to LG-EKF's ability to handle gimbal lock as explained in the next section.

2) Gimbal Lock: Next we investigate the impact of gimbal lock on the proposed approach. Any set of Euler angles will lose a degree of freedom when two of the rotation axes align [35], implying that in that configuration the rotation about the locked axis cannot be correctly estimated by EKF. Typically the order of the joint axes is carefully selected to try and avoid the lock, however in human motion estimation, gimbal lock often takes place at the shoulder joint due to its high manoeuvrability. Unlike the Euler angle formulation, an $\mathsf{SO}(3)$ representation of the spherical joint does not suffer from gimbal lock and thus LG-EKF will accurately estimate any rotation.

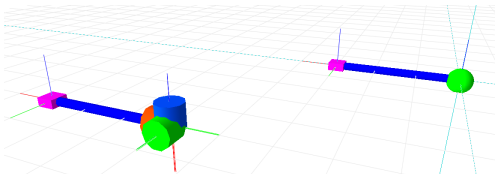

Fig. 5: Simulation model used for gimbal lock validation.

To demonstrate the benefits of LG-EKF over EKF during gimbal lock we simulate a single spherical joint at the origin with a single IMU attached at an offset of 0.1 meters in the x. The simulated model is shown in Fig. 5. A quintic polynomial is used to generate a smooth trajectory, sampling at 100 Hz. First, the model experiences a 1 second rotation about the world y axis with initial position 0 rads and final positions $\frac{\pi}{2}$ rads and zero initial and final velocity and acceleration. In the Euler angle model this motion aligns the first and third revolute joint axis putting it into a singularity and removing a degree of freedom (gimbal lock). Next, the model experiences the same 1 s rotation in the now locked world z axis. In order to focus only on the gimbal lock problem, no noise was added to the IMU measurements. Measurement noise, process noise, and initial covariances were set as described in Sec. V-A.1. Figure 6 shows the distance metric described in (31).

When Euler angles enter gimbal lock, the Euler angle based Jacobian is singular and thus the linearized system is no longer observable. In this case EKF cannot accurately estimate the states. By plotting the condition number of the observability matrix $\mathcal{O}_b = [\mathcal{H}_k\ \mathcal{H}_k\mathcal{F}_k\ \cdots]^T$ of the linearized system we can visualize the ability of the filters to handle gimbal lock (Fig. 7).

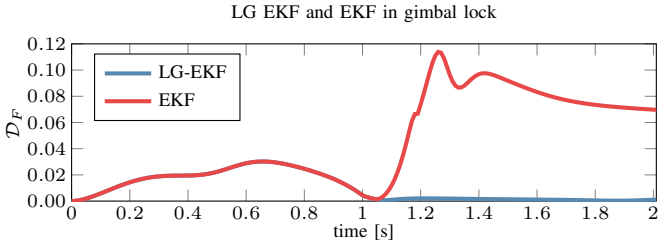

Fig. 6: LG-EKF and EKF estimation during gimbal lock. Both filters accurately estimate the rotation about the y axis until the system gets close to the gimbal lock, which happens at 1 second. After the rotation about y the Euler angle model is in gimbal lock and thus EKF cannot accurately track the orientation until the lock is escaped at 1.5 seconds. Once Euler angles escape the gimbal lock, EKF can regain an accurate estimate of the roll and pitch orientation using the accelerometer's gravity measurement. However, any error in yaw during gimbal lock accumulates. LG-EKF estimation is unaffected by gimbal lock.

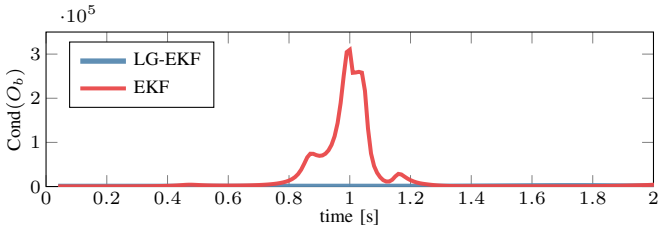

Fig. 7: Condition number of the observability matrix of the linearized system at each iteration during gimbal lock. The condition number of EKF increases rapidly from 0.75 seconds when the Euler angles are still 12° away from gimbal lock. In this region EKF may incorrectly estimate large state increments. LG-EKF retains observability during gimbal lock.

B. Real-world experiment

Using real human motion we verify that real human motion is better represented with the Lie Group motion model and that the proposed approach improves estimation throughout the state space and as well as near gimbal lock. We validate the proposed approach by comparing the distance between actual and estimated wrist and elbow positions during a dynamic figure eight human arm motion collected in a motion capture studio. The motion capture studio utilizes 8 Motion Analysis cameras capturing at 200Hz. Our IMUs are based on the MPU9250 sensor and were set to sample at 100Hz, they were calibrated with the algorithm proposed in [36] prior to data collection. The kinematic model of the participant was generated based on motion capture markers placed on the shoulder as well as medial and lateral sides of the elbow and wrist. Three motion capture markers were placed on each IMU to compute their offset and rotation from the humerus and radius.

For the best performance of both filters it is imperative to tune the initial covariance, observation noise, and process

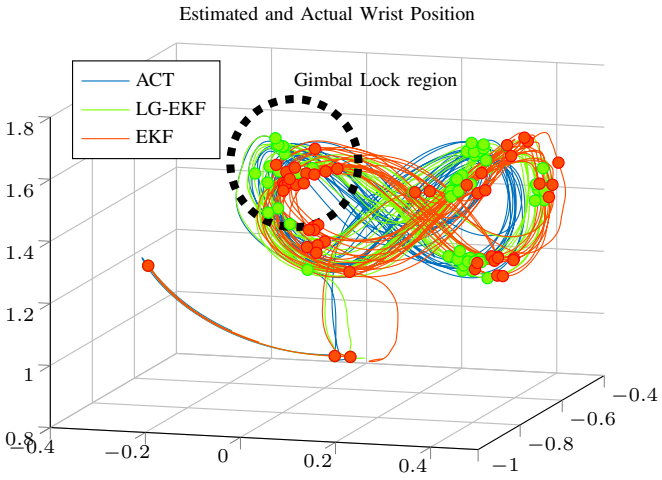

Fig. 8: Actual and estimated 3d wrist position.

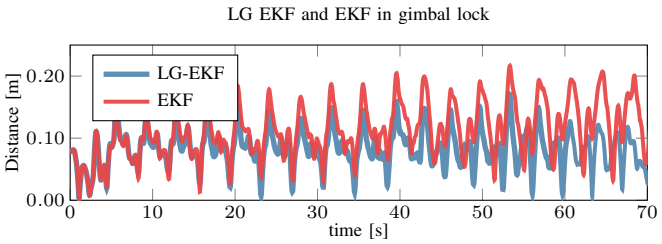

Fig. 9: Distance between the actual and estimated wrist positions. With each pass near gimbal lock, the Euler angle model EKF accumulates error about world Z axis.

noise parameters. In our experiment the initial pose of the participant is known and thus we set the initial covariance to 10^{-3} along the diagonal. The observation noise parameters are set to match those of the IMUs based on 30 seconds of static data. We assumed discrete constant acceleration process noise injection [29] of magnitude η as described in section V-A.1 and used the matlab optimization toolbox to find the optimal process noise parameter for EKF and LG-EKF such that the distance between the estimated and actual elbow and wrist positions is minimized over 3 repetitions of the figure eight motion. The optimal process noise parameters were found to be $\eta_{\text{EKF}} = 389.1$ and $\eta_{\text{LG-EKF}} = 264.8$ for EKF and LG-EKF respectively. The significantly lower optimal process noise for the Lie Group motion model shows that human motion is better estimated on the group.

Figure 8 shows the estimated and actual wrist positions for both EKF and LG-EKF. Figure 9 plots the distance between actual and estimated wrist positions. Both filters begin with equally accurate estimation, with each pass through the corner of the figure 8 near gimbal lock, EKF accumulates error about the world Z axis. Since LG-EKF is not affected by gimbal lock its performance stays consistent throughout the entire motion. Table I shows the RMSE and standard deviation for elbow and wrist position estimation.

TABLE I: Root mean squared error of estimated and actual elbow and wrist positions for the two filters. The proposed LG-EKF improves the position estimate by 30% over EKF.

	Elbow RMSE [cm]	Wrist RMSE [cm]
LG-EKF	**5.2 ± 2.6**	**6.9 ± 2.7**
EKF	7.4 ± 3.6	9.9 ± 3.8

VI. Conclusion

We proposed a novel algorithm for human motion estimation based on body worn IMU sensors. Based on the geometric arrangements of joints in the human body, we formed the state as a Cartesian product of Lie groups, namely the special orthogonal groups $\mathrm{SO}(2)$ and $\mathrm{SO}(3)$, which represent rotations in 2D and 3D, respectively. In order to stochastically infer the state of such a Lie group, we employed the LG-EKF, thus explicitly accounting for the non-Euclidean geometry of the state space. A constant acceleration motion model on the group was developed for the LG-EKF prediction step and the Jacobian of the IMU (gyroscope and accelerometer measurements), was derived for the update step. The performance of the proposed method was evaluated in both simulation and real-world data, comparing it with the EKF based on Euler angles. The proposed algorithm can estimate human motion with lower end effector position RMSE than the EKF and is not affected by gimbal lock.

References

[1] D. Kulić, G. Venture, K. Yamane, E. Demircan, I. Mizuuchi, and K. Mombaur, "Anthropomorphic movement analysis and synthesis: A survey of methods and applications," *IEEE Transactions on Robotics*, vol. 32, no. 4, pp. 776–795, 2016.

[2] V. Bonnet, C. Mazzà, J. McCamley, and A. Cappozzo, "Use of weighted fourier linear combiner filters to estimate lower trunk 3d orientation from gyroscope sensors data," *Journal of neuroengineering and rehabilitation*, vol. 10, no. 1, p. 29, 2013.

[3] X. Yun and E. R. Bachmann, "Design, implementation, and experimental results of a quaternion-based kalman filter for human body motion tracking," *IEEE transactions on Robotics*, vol. 22, no. 6, pp. 1216–1227, 2006.

[4] G. Ligorio and A. M. Sabatini, "A novel kalman filter for human motion tracking with an inertial-based dynamic inclinometer," *IEEE Transactions on Biomedical Engineering*, vol. 62, no. 8, pp. 2033–2043, 2015.

[5] H. Zhou, T. Stone, H. Hu, and N. Harris, "Use of multiple wearable inertial sensors in upper limb motion tracking," *Medical engineering & physics*, vol. 30, no. 1, pp. 123–133, 2008.

[6] T. Seel, J. Raisch, and T. Schauer, "Imu-based joint angle measurement for gait analysis," *Sensors*, vol. 14, no. 4, pp. 6891–6909, 2014.

[7] J. F. Lin and D. Kulić, "Human pose recovery using wireless inertial measurement units," *Physiological measurement*, no. 12, p. 2099, 2012.

[8] M. El-Gohary and J. McNames, "Shoulder and elbow joint angle tracking with inertial sensors," *Biomedical Engineering, IEEE Transactions on*, vol. 59, no. 9, pp. 2635–2641, 2012.

[9] A. Szczesna and P. Pruszowski, "Model-based extended quaternion kalman filter to inertial orientation tracking of arbitrary kinematic chains," *SpringerPlus*, vol. 5, no. 1, p. 1965, 2016.

[10] V. Joukov, B. Vincent, M. Karg, V. Gentiane, and D. Kulic, "Rhythmic ekf for pose estimation during gait," in *Humanoid Robots, 2016 IEEE-RAS*. IEEE, 2015.

[11] J. Ćesić, V. Joukov, I. Petrović, and D. Kulić, "Full body human motion estimation on lie groups using 3d marker position measurements," in *Humanoid Robots, 2016 IEEE-RAS*. IEEE, 2016, pp. 826–833.

[12] F. Su and C. Lee, "Uncertainty Manipulation and Propagation and Verification of Applicability of Actions in Assebly Tasks," in *International Conference on Robotics and Automation (ICRA)*, 1991, pp. 2471–2476.

[13] P. Smith, T. Drummond, and K. Roussopoulos, "Computing MAP trajectories by representing, propagating and combining PDFs over groups," in *International Conference on Computer Vision*, 2003, pp. 1275–1282.

[14] Y. Wang and G. S. Chirikjian, "Error propagation on the Euclidean group with applications to manipulator kinematics," *IEEE Transactions on Robotics*, vol. 22, no. 4, pp. 591–602, 2006.

[15] A. Long, K. Wolfe, M. Mashner, and G. S. Chirikjian, "The Banana Distribution is Gaussian: A Localization Study with Exponential Coordinates." in *Robotics, Science and Systems*, 2012, p. 8.

[16] T. D. Barfoot and P. T. Furgale, "Associating uncertainty with three-dimensional poses for use in estimation problems," *IEEE Transactions on Robotics*, vol. 30, no. 3, pp. 679–693, 2014.

[17] C. Forster, L. Carlone, F. Dellaert, and D. Scaramuzza, "IMU Preintegration on Manifold for Efficient Visual-Inertial Maximum-a-Posteriori Estimation," in *Robotics: Science and Systems*, 2015, p. 9.

[18] G. Bourmaud, R. Mégret, A. Giremus, and Y. Berthoumieu, "Discrete Extended Kalman Filter on Lie Groups," in *European Signal Processing Conference (EUSIPCO)*, 2013, pp. 1–5.

[19] G. Bourmaud, R. Mégret, M. Arnaudon, and A. Giremus, "Continuous-Discrete Extended Kalman Filter on Matrix Lie Groups Using Concentrated Gaussian Distributions," *Journal of Mathematical Imaging and Vision*, vol. 51, no. 1, pp. 209–228, 2015.

[20] G. Bourmaud, R. Mégret, A. Giremus, and Y. Berthoumieu, "From Intrinsic Optimization to Iterated Extended Kalman Filtering on Lie Groups," *Journal of Mathematical Imaging and Vision*, vol. 55, no. 3, pp. 284–303, 2016.

[21] Y. Bar-Shalom, X. R. Li, and T. Kirubarajan, *Estimation with Applications To Tracking and Navigation*. John Wiley & Sons, Inc., 2001, vol. 9.

[22] J. Ćesić, I. Marković, and I. Petrović, "Moving object tracking employing rigid body motion on matrix Lie groups," in *19th International Conference on Information Fusion (FUSION), Special Session on Directional Estimation*, 2016, p. 7.

[23] J. Stillwell, *Naive Lie Theory*. Springer, 2008.

[24] J. M. Selig, "Lie Groups and Lie Algebras in Robotics," in *Computational Noncommutative Algebra and Applications*, 2005, pp. 101–125.

[25] W. Park, Y. Wang, and G. S. Chirikjian, "The Path-of-Probability Algorithm for Steering and Feedback Control of Flexible Needles," *The International Journal of Robotics Research*, vol. 29, no. 7, pp. 813–830, 2010.

[26] K. Tapp, *Matrix Groups for Undergraduates*. American Mathematical Society, 2005.

[27] Y. Wang and G. S. Chirikjian, "Nonparametric Second-Order Theory of Error Propagation on Motion Groups," *The International Journal of Robotics Research*, vol. 27, no. 11, pp. 1258–1273, 2008.

[28] G. S. Chirikjian, *Stochastic Models, Information Theory, and Lie Groups, Volume 2: Analytic Methods and Modern Applications*. Springer, 2012.

[29] Y. Bar-Shalom, T. Kirubarajan, and X.-R. Li, *Estimation with Applications to Tracking and Navigation*. John Wiley & Sons, Inc., 2002.

[30] M. W. Spong, S. Hutchinson, and M. Vidyasagar, *Robot Modeling and Control*. John Wiley & Sons, Inc., 2006.

[31] J. Ćesić, I. Marković, I. Cvišić, and I. Petrović, "Radar and stereo vision fusion for multitarget tracking on the special Euclidean group," *Robotics and Autonomous Systems*, 2016.

[32] V. Joukov, J. Ćesić, K. Westermann, I. Marković, D. Kulić, and I. Petrović, "Supplementary material to Human motion estimation on Lie groups using IMU measurements," 2017. [Online]. Available: https://ece.uwaterloo.ca/~dkulic/pubs/JoukovIROS2017Supplementary.pdf

[33] V. Joukov, M. Karg, and D. Kulić, "Online tracking of the lower body joint angles using imus for gait rehabilitation," in *IEEE Engineering in Medicine and Biology Conference*, Aug 2014, pp. 2310–2313.

[34] D. Q. Huynh, "Metrics for 3d rotations: Comparison and analysis," *Journal of Mathematical Imaging and Vision*, vol. 35, no. 2, pp. 155–164, 2009.

[35] F. S. Grassia, "Practical parameterization of rotations using the exponential map," *Journal of graphics tools*, vol. 3, no. 3, pp. 29–48, 1998.

[36] D. Tedaldi, A. Pretto, and E. Menegatti, "A robust and easy to implement method for imu calibration without external equipments," in *ICRA*. IEEE, 2014, pp. 3042–3049.